NMR and NQR Studies of Borate Glasses*

Philip J. Bray and Gary L. Petersen**

Department of Physics, Box 1843, Brown University, Providence, Rhode Island 02912

Z. Naturforsch. **53 a,** 273–284 (1998); received December 30, 1997

Nuclear magnetic resonance (NMR) has been used for some 40 years to study atomic arrangements, chemical bonding, and structural groupings in borate glasses and crystalline compounds, and nuclear quadrupole resonance (NQR) has more recently increased the resolution and accuracy of the measurements. Examples are presented of the use of first-order and second-order quadrupolar effects in ^{11}B NMR spectra to obtain structural information, and ^{11}B and ^{10}B NQR spectra to obtain the quadrupolar parameters Q_{cc} (the coupling constant) and η (the asymmetry parameter) with accuracies of 5 or 6 significant figures, and 3 figures, respectively. Q_{cc} and η are extremely sensitive to changes in atomic rearrangements and chemical bonds, so they are excellent monitors and provide identification of bonding configurations and structural groupings in borates: Examples are also presented in which combinations of NMR and NQR data are used to extract the desired information. NQR detection of resonances at frequencies as low as 276 kHz is discussed.

Key words: NMR; NQR; Borates; Quadrupolar Interactions.

Introduction

NMR has been employed for some 40 years or so [1] to study structure and chemical bonding in borate glasses, and NQR methods have recently [2 - 6] expanded these studies. The present paper presents examples of the use of both techniques to obtain the quadrupolar parameters Q_{cc} and η for the ^{11}B and ^{10}B isotopes in these glasses, where Q_{cc} is the quadrupolar coupling constant $e^2V_{zz}Q$ and $\eta = (V_{xx} - V_{yy})/V_{zz}$; here the V_{ii} are the components of the electrical field gradient (EFG) tensor at the nuclear site in its system of principal axes and Q is the electrical quadrupole moment of the nucleus. Since the V_{ii} are extremely sensitive to changes in the atomic positions and the chemical bondings in a material, the values of Q_{cc} and η are excellent monitors of those characteristics. Also presented are cases in which combined NMR and NQR data can be used to extract the desired information.

* Presented at the XIVth International Symposium on Nuclear Quadrupole Interactions, Pisa, Italy, July 20–25, 1997.

** President, RITEC, Inc., 60 Alhambra Road, Suite 5, Warwick, RI USA 02886

Reprint requests to Prof. P. J. Bray; Fax: 401-863-2024, E-mail: bray@physics.brown.edu.

NMR Spectroscopy

Figure 1 displays the theoretical NMR response pattern (without inclusion of broadening mechanisms) for a spin I = 3/2 nucleus (e. g. ^{11}B) in a glass or polycrystalline powder [7]. The case considered is that of a quadrupolar interaction sufficiently small to be handled as a first-order perturbation of the NMR energy levels set up by the Zeeman interaction of the nuclear magnetic moment with an applied magnetic field. The symbol ν_Q in the figure is just $Q_{cc}/2$ for a nucleus of spin 3/2. Note that the "central" transition (m = +1/2 $\leftrightarrow$ m = –1/2, where m is the magnetic quantum number) is not affected by the first-order perturbation, and that the "satellite" transitions (+3/2 to + 1/2, and –3/2 to –1/2) are spread out into a characteristic "powder pattern" with divergences and shoulders symmetrically located about the Larmor frequency ν_0 (i. e. the NMR frequency in the absence of any perturbations of the Zeeman energy levels).

Figure 2 is the ^{11}B NMR response for a polycrystalline powder of lithium diborate ($Li_2O{\cdot}2B_2O_3$) obtained [2] at a frequency of 96.3 MHz employing a magnetic field of 7.1 Tesla. (The central response would rise to a distance of some 30 to 40 times the height of the figure if it were not cut off.) The divergences and one set of shoulders are apparent.

0932-0784 / 98 / 0600-0273 $ 06.00

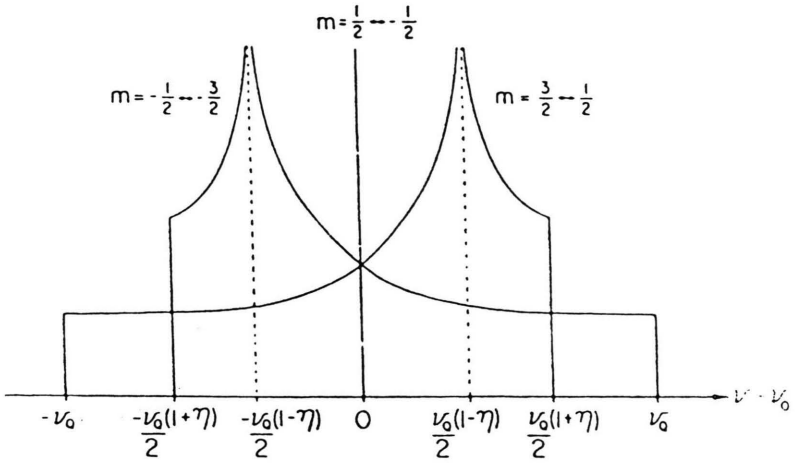

Fig. 1. Theoretical NMR spectrum (without broadening interactions) for a nucleus with spin I = 3/2 and a first-order quadrupolar interaction.

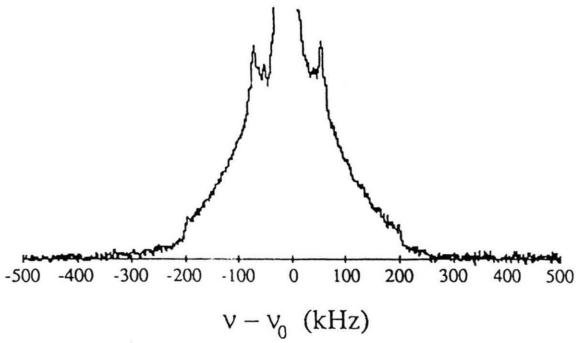

Fig. 2. NMR spectrum at 96.3 MHz for ^{11}B in powdered crystalline lithium diborate at 7.1 Tesla.

Additional studies at lower frequencies have confirmed the identification of the detected shoulders as the inner shoulders of Fig. 1 at $\pm\frac{1}{4}Q_{cc}(1+\eta)$ rather than the outer shoulders at $\pm Q_{cc}/2$. The latter are not detected because of the severe fall off of the power level as one moves out in frequency from ν_0 in the pulsed spectrometer employed for this study. Vestiges may be seen at approximately ±263 kHz, but they are unusable for calculations of Q_{cc} and η. This material contains both 3-coordinated borons (bonded to three oxygens in triangular BO_3 configurations) and 4-coordinated borons (bonded to four oxygens in tetrahedral BO_4 configurations). The first-order pattern in Fig. 2 arises from the 4-coordinated borons for which the quadrupolar parameters are found to be Q_{cc} = 527±6 kHz and η = 0.53±0.03. For all borates studied to date, the value of Q_{cc} for 4-coordinated borons is less than 1 MHz, but η can have any value between 0 and 1. Extraction [2, 8] of values of Q_{cc} and η for the 3-coordinated borons in $Li_2O{\cdot}2B_2O_3$ will be discussed later in this paper.

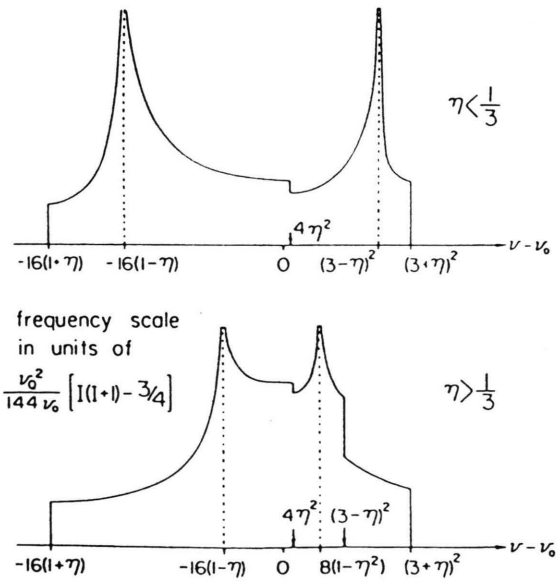

Fig. 3. Theoretical NMR spectrum (without broadening interactions) for the central transition ($m = -1/2 \leftrightarrow m = +1/2$) of half-integer spin nuclei with a second-order quadrupolar interaction. $\nu_Q = Q_{cc}/2$ for spin I = 3/2. The position marked 0 is the Larmor frequency ν_0.

When the quadrupolar interaction is sufficiently large to require treatment as a second-order perturbation of the Zeeman interaction, the central transition (–1/2 ↔ +1/2) is affected [9] and is spread out into the pattern displayed (without inclusion of broadening mechanisms such as the dipole - dipole interaction) in Figure 3. (Here again $\nu_Q = Q_{cc}/2$ for spin I = 3/2). For this case of a larger quadrupolar interaction, the satellite transitions are generally spread out over a very large frequency range and are not

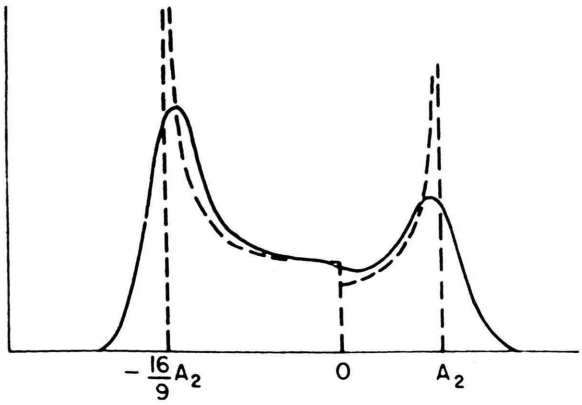

Fig. 4. Resonance lineshape without (dashed lines) and with (solid curve) broadening interactions for the case (Fig. 3) of a second-order quadrupolar interaction with $\eta = 0$. Here $A_2 = \frac{3}{64}Q_{cc}/\nu_0$.

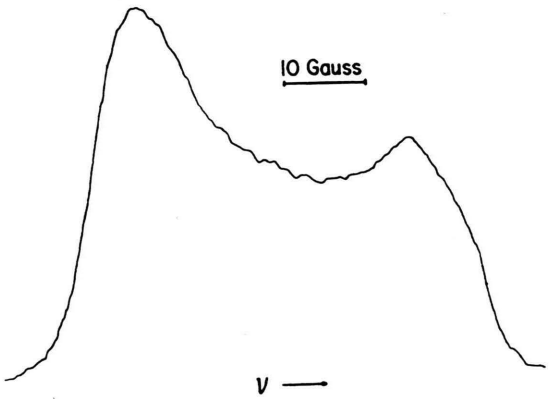

Fig. 5. ^{11}B NMR spectrum of vitreous B_2O_3 at ν_0 = 16 MHz.

detected without special effort. Generally, only the central transition is recorded but, fortunately, comparison of computer-generated spectra with the actual spectrum yields values for both Q_{cc} and η. An illustrative example of this case for a very small or vanishing value of η is provided by vitreous boron oxide (B_2O_3). First, consider Fig. 4 where the dashed lines give the powder pattern shown in Fig. 3, but for small or vanishing η, and the solid line includes the effects of broadening mechanisms. Figure 5 is the ^{11}B NMR spectrum obtained at ν_0 = 16 MHz for the B_2O_3 glass. Figure 6 displays the first derivative of the same resonance obtained at ν_0 = 8 MHz, along with a superimposed computer-generated spectrum using Q_{cc} = 2.64 MHz and η = 0.12 with distribution

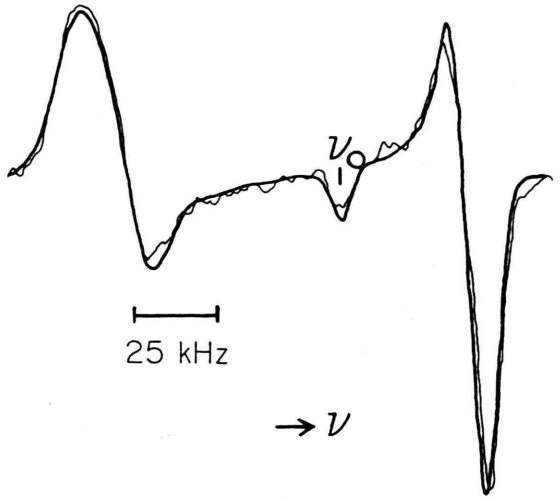

Fig. 6. Experimental ^{11}B derivative spectrum for vitreous B_2O_3, and a superimposed computer generated spectrum using the values of the quadrupolar parameters given in the text.

parameters $\sigma_{Q_{cc}} = 0.10$ MHz and $\sigma_\eta = 0.043$. (The distributions, which are in the components of the EFG tensor, arise from the relative structural disorder in a glass as compared to a crystalline material.) (The first derivative of the absorption curve is the spectrum yielded by many NMR spectrometers, and has proved to be much more sensitive than the absorption curve in revealing weak or subtle features in the spectrum). Vitreous B_2O_3 is composed principally of boroxol groups (see Figure 7). The values of Q_{cc} for 3-coordinated borons in all borates studied to date lie between 2.4 and 2.9 MHz. Clearly, NMR spectra distinguish very clearly between 4-coordinated and 3-coordinated borons.

When a metal oxide (e. g. alkali or alkaline earth oxide) is added to B_2O_3, two things may happen: formation of 4-coordinated borons, (i.e. the boron obtains an extra electron from the metal ion and uses it to bond to a fourth oxygen) or formation of nonbridging oxygens (NBO) in BO_3 configurations (i. e. one or more of the oxygens in the BO_3 unit obtains an extra electron and does not bond with another boron). In the latter case, the (exact or approximate) 3-fold axis of symmetry through the boron in the triangular BO_3 unit is lost (unless there are 3 NBO) because the oxygens are no longer equivalent. One expects a large asymmetry parameter, and Fig. 8a displays [10] an (unbroadened) powder pattern like that shown in the lower portion of Fig. 3. When broadening is included, and the derivative is taken, the spectrum in

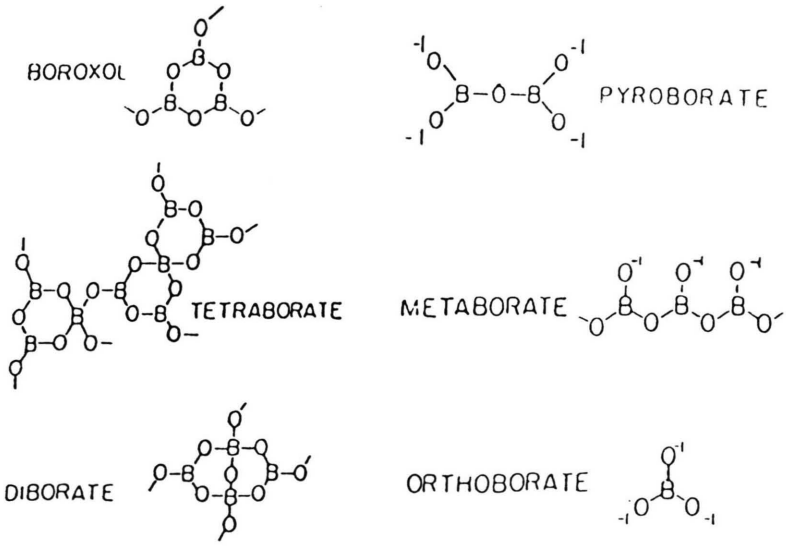

Fig. 7. Some of the structural groupings found in alkali borate compounds and glasses.

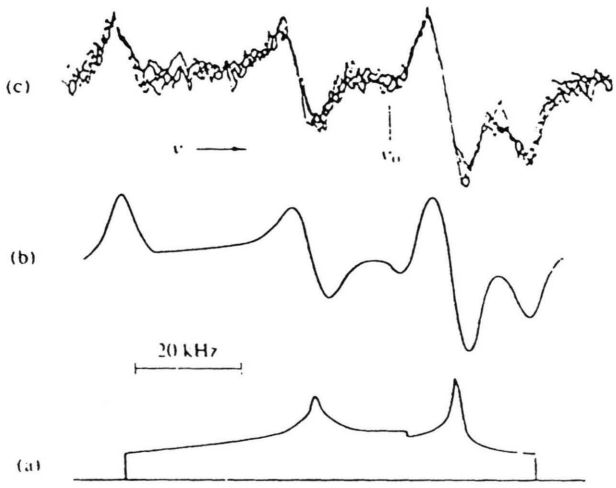

Fig. 8. (a) Theoretical powder pattern for the central ($m = -1/2 \leftrightarrow m = +1/2$) transition with $I = 3/2$, $\nu_0 = 16$ MHz, $Q_{cc} = 2.56$ MHz, and $\eta = 0.54$. (b) First derivative of the theoretical powder pattern after convolution with a Gaussian curve of linewidth $\sigma = 2.5$ kHz. (c) Superposition of four experimental traces for ^{11}B in polycrystalline calcium metaborate, at a resonant frequency of 16 MHz.

Fig. 8b is generated by the computer. Figure 8c displays a superposition of the computer-generated and experimental [10] spectra for ^{11}B in calcium metaborate ($CaO{\cdot}B_2O_3$) which has the chain structure displayed in Figure 7. The quadrupolar parameters obtained from the best fit of the computer-generated spectrum to the recorded response are $Q_{cc} = 2.56$ MHz and $\eta = 0.54$. Similar spectra and quadrupolar parameters have been found for other metaborates (1 NBO) and pyroborates (2 NBO), but the orthoborates (3 NBO) have spectra similar to that of vitreous B_2O_3 (Fig. 5) with small η values because the (approximate) 3-fold symmetry is present. For all three cases (1, 2, or 3 NBO) the values of Q_{cc} are again between 2.4 and 2.9 MHz, but whereas η is less than 0.20 for all of the BO_3 units with zero or three NBO, it is always greater than 0.40 for the non-symmetric BO_3 (i.e. 1 or 2 NBO). NMR clearly distinguishes between symmetric and non-symmetric BO_3 configurations.

The generally accepted model for borate glasses is that of Jan Krogh-Moe [11] in which the glasses consist of a mixture of the structural groupings found in the crystalline compounds of the glassforming system. (Some of these are shown in Figure 7). In general, then, the ^{11}B NMR spectrum for a borate glass will contain responses from 4-coordinated borons, and 3-coordinated borons with 0, 1, 2, 3 NBO. This situation is shown in Fig. 9 where the first derivative of the absorption curve for a characteristic borate glass is displayed at the top of the figure. Fittings to computer-generated spectra can obtain the quadrupolar parameters and relative amounts of each type of

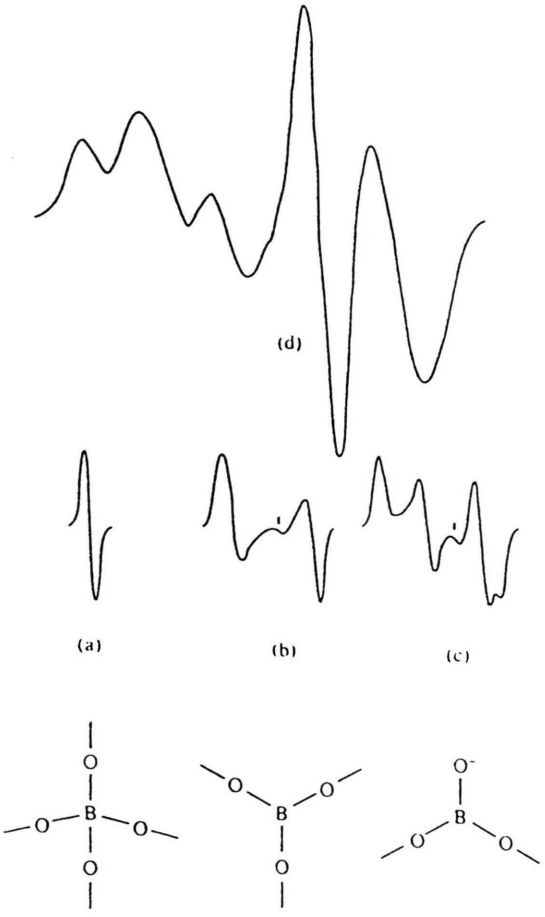

Fig. 9. ^{11}B NMR spectrum of (a) a BO_4 unit, (b) a BO_3 unit with all bridging [or all non-bridging] oxygens (NBO), (c) a BO_3 unit with one NBO [or two NBO], and (d) a sample containing units of type (a), (b), and (c).

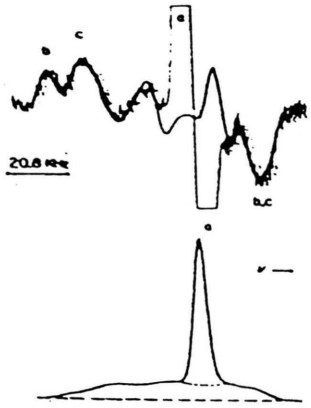

Fig. 10. The ^{11}B NMR spectrum for a sodium borosilicate glass of molar composition 1.3 $Na_2O{\cdot}B_2O_3{\cdot}SiO_2$: bottom, the absorption response; top, the first derivative response.

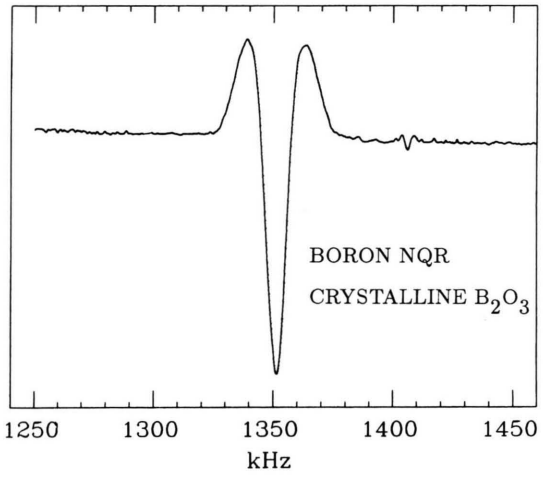

Fig. 11. Partial boron NQR spectrum of crystalline B_2O_3.

boron-oxygen configuration, and matching of the parameters to those of the crystalline compounds can identify the structural groupings that are present. The absorption spectrum for an actual sodium borosilicate glass [12] is displayed in Fig. 10, along with its first derivative. (This is a striking example of the greater sensitivity of the derivative spectrum to features of the absorption spectrum.) It is clear that one can run into problems disentangling the responses from the various boron-oxygen configurations, since they are all superimposed on top of each other, and weak responses may actually be lost completely. A way to separate the responses from each other would be extremely useful, and nuclear quadrupole resonance (NQR) spectroscopy can do just that.

NQR Spectroscopy

In NQR spectroscopy, no magnetic field is used to generate Zeeman energy levels. The levels are set up by the electrical quadrupole interaction itself, and transitions between the levels are stimulated as in NMR spectroscopy. For the case of a spin $I = 3/2$ nucleus there is just one transition frequency [13] given by

$$\nu_0 = \frac{Q_{cc}}{2}\sqrt{1+\frac{\eta^3}{3}}, \tag{1}$$

since the $m = \pm 3/2$ energy levels are degenerate (i. e. identical) as are the $m = \pm 1/2$ levels. Since the

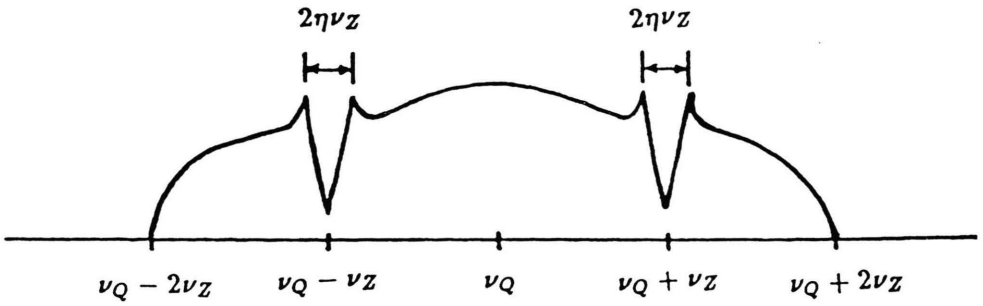

Fig. 12. NQR response for a nucleus of spin $I = 3/2$ with a small magnetic field applied parallel to the axis of the coil containing the sample.

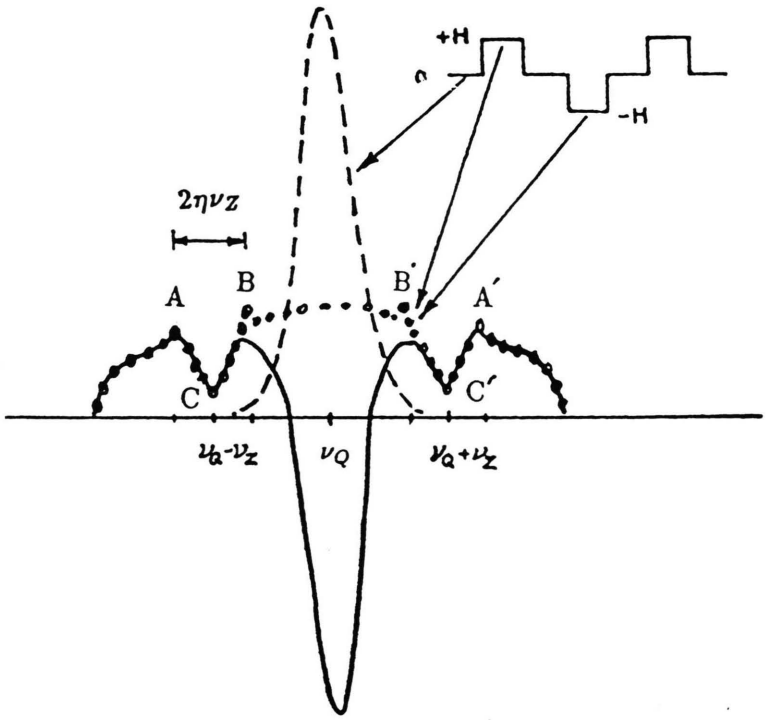

Fig. 13. NQR lineshape obtained using a square wave Zeeman modulation. The resonance obtained when the modulation field is off is indicated by the broken line; the powder pattern appears (circles) when the field is on; the detected response (solid line) is the difference between the broken line and the line of circles.

Q_{cc} values are less than 3 MHz for ^{11}B in borates (and can be values down to zero for 4-coordinated borons), a spectrometer is needed that can operate with very high sensitivity at frequencies that are below about 1.7 MHz. Such spectrometers have now been constructed [2].

Figure 11 displays the ^{11}B NQR response [2] for crystalline boron oxide (B_2O_3). This single response, obtained at 77 K, is near 1.35 MHz. (The much smaller response near 1.4 MHz will be discussed later). Since there is only one ^{11}B transition whose frequency is given by (1), it is not possible to extract values for Q_{cc} and η. But application of a small magnetic field (e. g. 30 gauss) along the axis of the radiofrequency coil containing the sample changes the response pattern to that shown in Fig. 12, where ν_z is just the product of the known gyromagnetic ratio of the nucleus and the strength of the applied magnetic field. Recognition of the features in the pattern clearly permits extraction of the value of η; (1) then yields Q_{cc}.

It is not necessary to apply a constant field, and advantage can be taken of the need to provide some type of modulation so that an audio signal is available for amplification and lock-in detection. Figure 13 displays [14, 15] the antisymmetric square wave of a

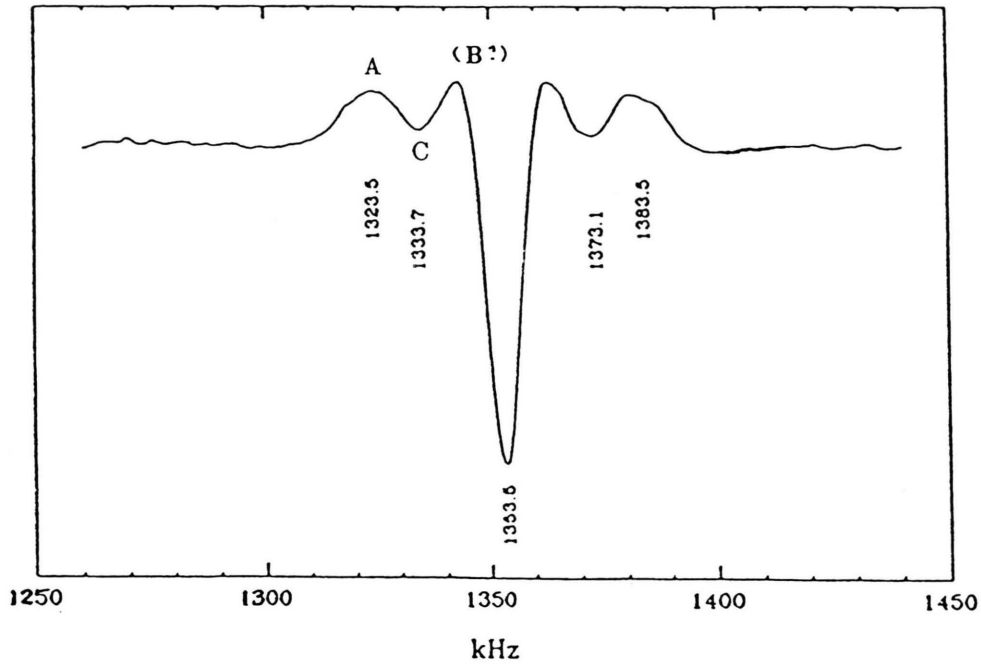

Fig. 14. ^{11}B NQR response obtained for $CaO{\cdot}B_2O_3$ using Zeeman square wave modulation. The sharp features in Fig. 12 are smoothed by broadening interactions.

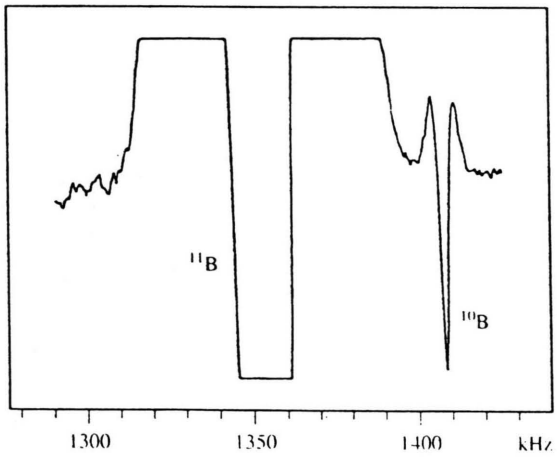

Fig. 15. The features of Fig. 11 displayed with a greatly expanded vertical scale.

magnetic field that is actually applied along the axis of the sample-containing coil. (The antisymmetric character blocks the generation of a false audio signal at the fundamental frequency of the modulation.) When the field is off, the dashed response is achieved, but the dotted curve (as in Fig. 12) is generated when the field is on. The circuitry places the two signals 180° out of phase so that the solid line depicts the actual response. An actual recorded response [14] for ^{11}B in polycrystalline $CaO{\cdot}B_2O_3$ at 77K is displayed in Figure 14. Values of Q_{cc} and η are obtained whose accuracy is comparable to that achieved in analysis of the second-order response pattern (e. g. Fig. 8) in NMR.

Fortunately, much more accurate values of the quadrupolar parameters can be achieved using NQR responses of the ^{10}B isotope. One of those is visible (as noted earlier) near 1.4 MHz in Fig. 11 for polycrystalline B_2O_3. A vertically expanded recording of that case is shown in Figure 15. But there can be as many as 13 such responses [16] for this spin $I = 3$ nucleus, as shown in Fig. 16 where the quantity ν/Q_{cc} is plotted against η where ν is the measured frequency of one of the ^{10}B responses. Proper identification of two or more of the possible resonances can be used to determine the value of η from Fig. 16; the ratio of the frequencies facilitates this process. And then the values of ν and η yield Q_{cc}. Computer programs are available that accept the measured frequencies and yield directly the values of Q_{cc} and η. Figure 17 displays another [2] of the ^{10}B responses from crystalline B_2O_3; most of the others have also been detected. Table 1 contains a summary of Q_{cc} and η values for

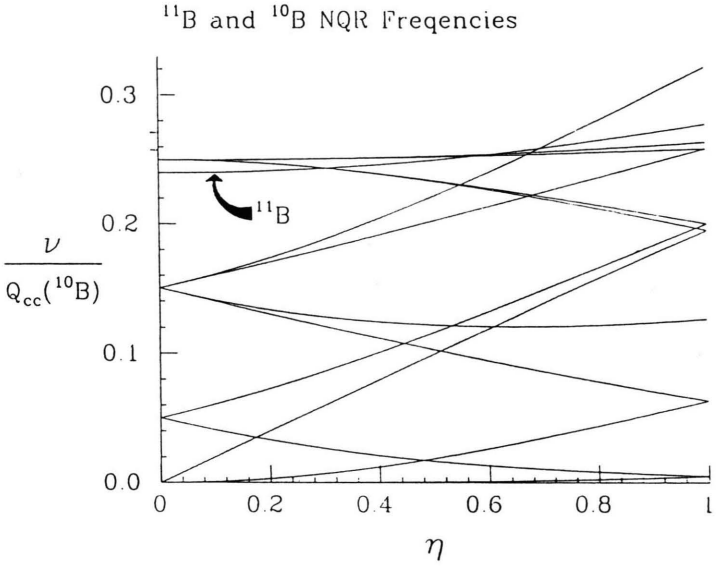

Fig. 16. ^{10}B (spin $I = 3$) NQR frequencies (in units of Q_{cc} for ^{10}B) plotted against the asymmetry parameter η. The single ^{11}B frequency is also shown.

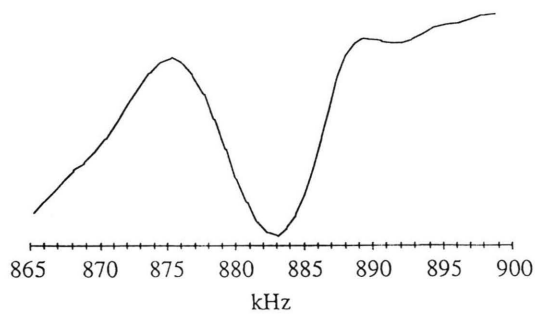

Fig. 17. One of the ^{10}B NQR responses for crystalline B_2O_3.

this material at 77 K, and one will notice that ^{10}B NQR characteristically yields 5-figure accuracy for Q_{cc} and 3-figure accuracy for η while NMR gives 3 and 2 figures, respectively.

Figure 18 displays [14] some of the ^{10}B NQR responses for polycrystalline $CaO{\cdot}B_2O_3$ at 77 K. (The weaker responses have been confirmed by multiple runs and/or an increase in the signal averaging time). Table 2 presents a comparison of the experimental and calculated ^{10}B response frequencies when the values $Q_{cc} = 2594.30\pm0.05$ kHz and $\eta = 0.515\pm0.001$ are employed. An attempt was made to secure the ^{10}B signals at room temperature using all of the same spectrometer parameters and settings, but they were not detected. However, the single strong ^{11}B response was available near 1.34 MHz. Resort was then had to high-field NMR which yielded the responses [14] shown in Fig. 19, where the location of the divergences in the powder pattern is obvious (see Figure 1).

Table 1. ^{11}B quadrupole parameter in B_2O_3.

	NMR 300 K	NQR 300 K	NQR 77 K
Q_{cc} (kHz)	2690±30	2682.6±0.5	2701.1±0.2
η	0.06±0.02	0.071±0.001	0.067±0.001

Table 2. Experimental and theoretical ^{11}B and ^{10}B lines in $CaO\text{-}B_2O_3$; the ^{10}B line with an * is a "multi-quantum transition".

kHz	Experimental	Calculation
^{11}B	1353.3±0.5	1353.5±0.5
^{10}B	1368.6±0.2	1368.0±0.8
^{10}B	1363.7±0.3	1364.1±0.8
^{10}B	1359.8±0.2	1359.5±1.5
^{10}B	1355.4±0.2	1355.6±1.5
^{10}B	1209.9±0.2	1210.6±1.8
^{10}B*	1188.8±0.2	1189.3±1.0
^{10}B	1101.3±0.2	1102.0±1.3
^{10}B	657.4±0.2	657.8±0.7
^{10}B	639.4±0.2	640.0±1.8
^{10}B	552.2±0.2	552.8±2.2
^{10}B	549.8±0.2	549.3±1.2

Combining the NQR and NMR data, one obtains (see (1) and Fig. 1)

$$\frac{Q_{cc}}{2}\sqrt{1+\frac{\eta^3}{3}} = 1341.6 \pm 0.05\,\text{kHz},$$

$$\frac{Q_{cc}}{2}(1-\eta) = 621.3 \pm 0.5\,\text{kHz},$$

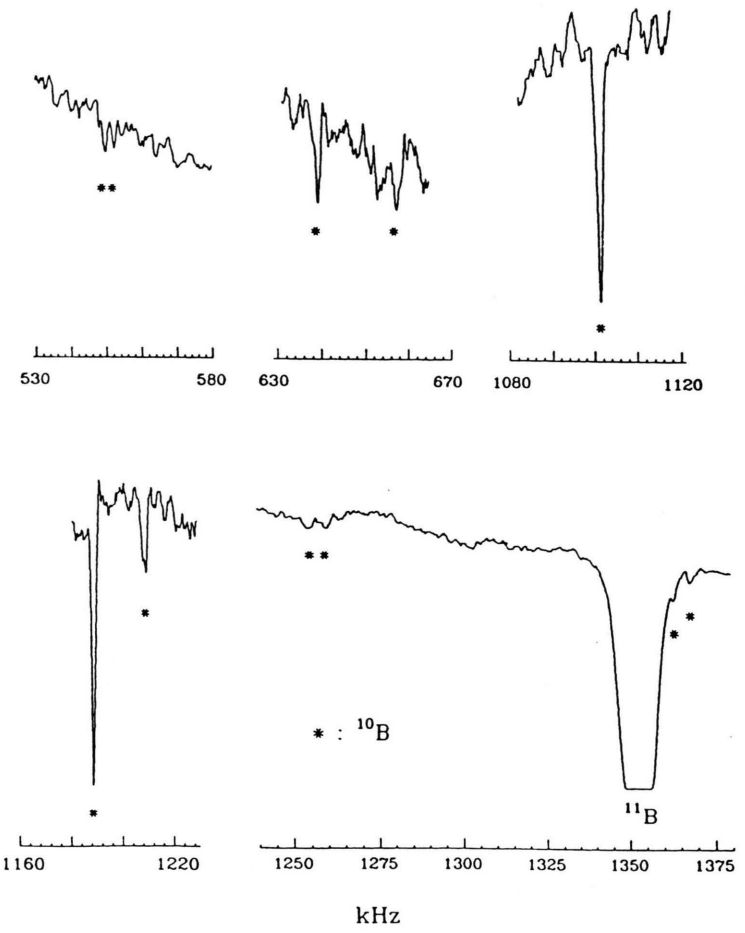

Fig. 18. The ^{11}B and ^{10}B NQR spectra of $CaO{\cdot}B_2O_3$ at 77K. The ^{11}B response is driven off scale in order to show the ^{10}B lines.

yielding $Q_{cc} = 2573.5 \pm 0.5$ kHz and $\eta = 0.511 \pm 0.002$. The change in Q_{cc} between 77K and about 300K is only some 0.8%.

So far only NQR responses from 3-coordinated borons have been presented. Figure 20 displays the ^{11}B NQR response [2, 6] near 276 kHz at 77K from the 4-coordinated borons in $Li_2O{\cdot}2B_2O_3$. When this result is combined with the data from the NMR spectrum for this material in Fig. 2, the quadrupolar parameters quoted earlier are obtained (Q_{cc} = 527±6 kHz and η = 0.53±0.03). It should be noted that the first-order satellite transitions (which go as Q_{cc}) for the 3-coordinated borons in this material are spread out so far in Fig. 2 (because Q_{cc} = 2622.5±0.2 kHz at 77 K) that they are not observable in the figure, and the second-order quadrupolar effects (which go as Q_{cc}^2/ν_o) on the central transition for those borons are so reduced at ν_o = 96.3 MHz that they are concealed within the narrow central response in Fig. 2 that arises from the central transitions for both the 3-coordinated and 4-coordinated borons. (For completeness, the value of $\eta = 0.1653 \pm 0.0007$ at 77 K is noted here for the 3-coordinated borons in this material.) The 276 kHz location of the ^{11}B response from the 4-coordinated borons in $Li_2O{\cdot}2B_2O_3$ is the lowest frequency to date at which boron NQR has detected a resonance. Below roughly that frequency, the well-known $1/f$ noise generated in the circuit components (where f is the spectrometer frequency) causes the noise to blow up and conceal possible responses.

Another successful detection of ^{11}B NQR responses from 4-coordinated borons [17] is depicted in Fig. 21 for polycrystalline lead diborate ($PbO{\cdot}2B_2O_3$). There are two boron sites in this material in which all borons are 4-coordinated because of the presence of sufficient 3-coordinated oxygens. (Normally, there are equal numbers of 3 and 4-coordinated borons in diborates; see, for example,

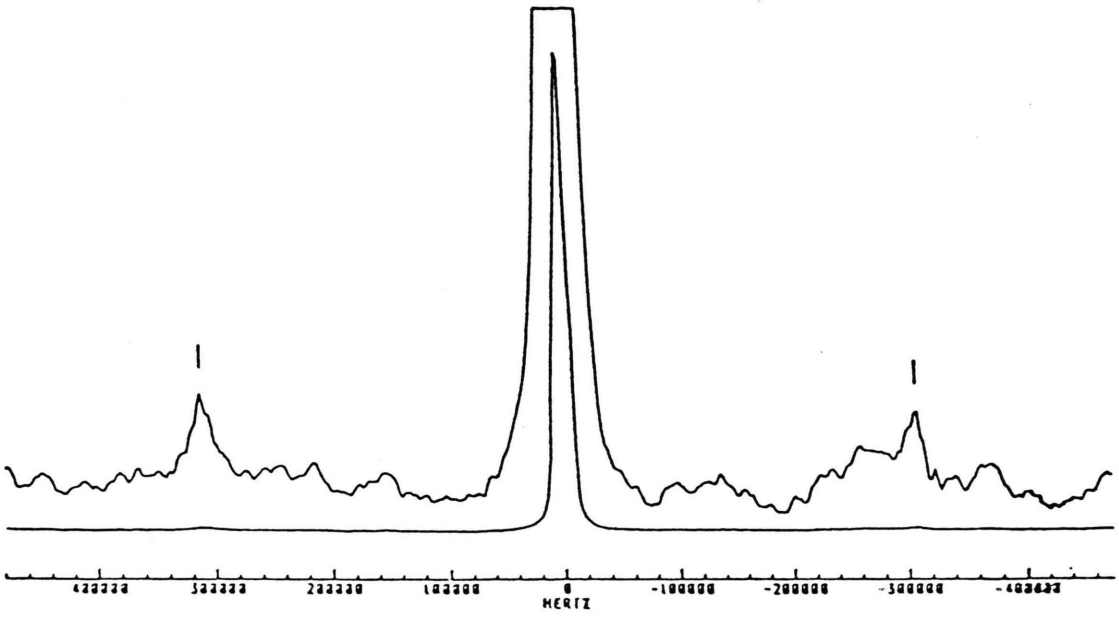

Fig. 19. First-order quadrupolar powder pattern at room temperature for $CaO{\cdot}B_2O_3$ at 96.3 MHz: the trace on the top is a greatly vertically expanded version of the bottom one; the marked peaks are the divergences of the satellite transitions.

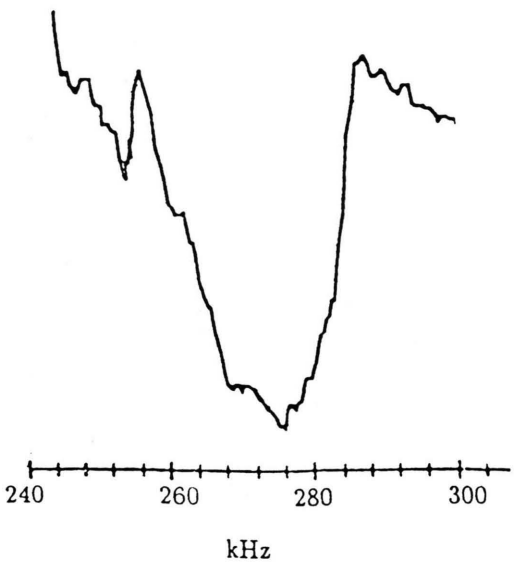

Fig. 20. The 276 kHz ^{11}B NQR response for four-coordinated borons in polycrystalline $Li_2O{\cdot}2B_2O_3$ at 77K.

the diborate structural grouping in Fig. 7). The two ^{11}B peaks are in the 400 - 500 kHz range, but ^{10}B responses have not yet been detected. Again, resort was had to the NMR spectrum for this material [17] which is displayed in Fig. 22, where the divergences in the first-order satellite transitions (see Fig. 1) are observable. Combination of the NQR and NMR data yields

$$\frac{Q_{cc}}{2}\sqrt{1+\frac{\eta^3}{3}} = 403.2 \pm 0.5\,\text{kHz},$$

$$\frac{Q_{cc}}{2}(1-\eta) = 361 \pm 2\,\text{kHz},$$

for one BO_4 site, and

$$\frac{Q_{cc}}{2}\sqrt{1+\frac{\eta^3}{3}} = 478.8 \pm 0.5\,\text{kHz},$$

$$\frac{Q_{cc}}{2}(1-\eta) = 452 \pm 2\,\text{kHz},$$

for the other BO_4 site, from which one obtains

$$Q_{cc} = 805 \pm 5\ \text{kHz},\ \eta = 0.09 \pm 0.03$$

for site 1, and

$$Q_{cc} = 960 \pm 5\ \text{kHz},\ \eta = 0.05 \pm 0.03$$

for site 2.

It was noted earlier (see Fig. 5) that only one boron site is apparent from the ^{11}B NMR spectrum for

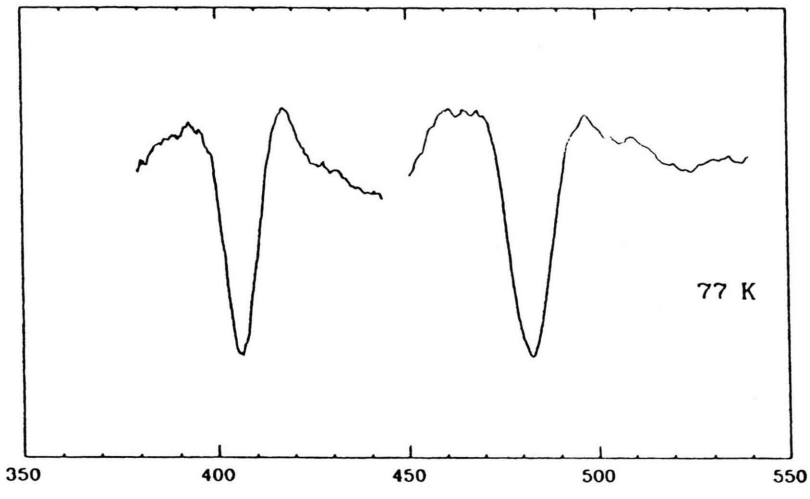

Fig. 21. ^{11}B NQR responses of polycrystalline $PbO{\cdot}2B_2O_3$ at 77K.

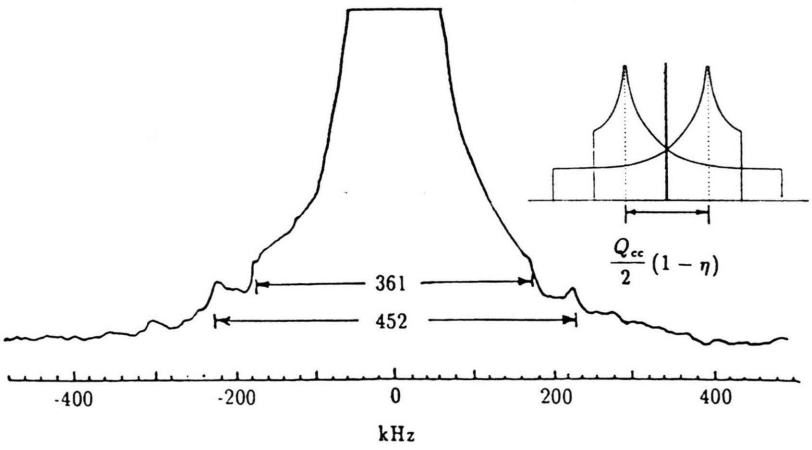

Fig. 22. ^{11}B NMR spectrum of $PbO{\cdot}2B_2O_3$ at 96.3 MHz.

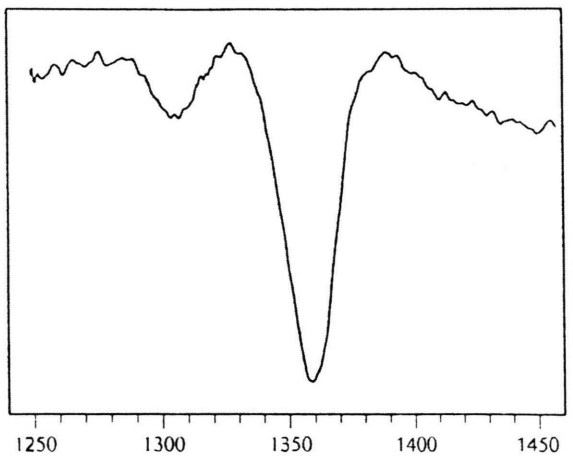

Fig. 23. ^{11}B NQR responses from vitreous B_2O_3.

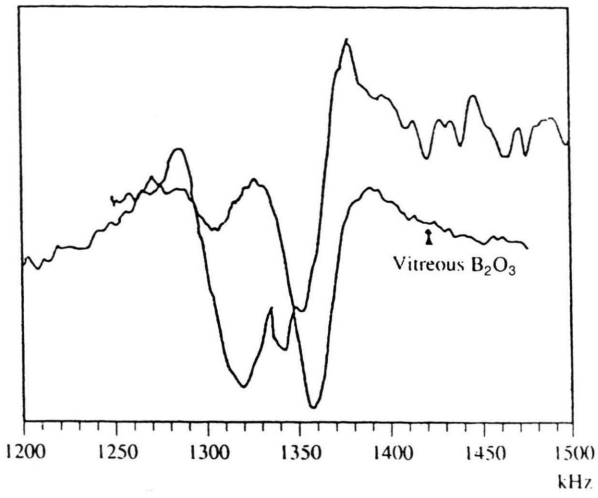

Fig. 24. ^{11}B NQR spectrum of a glass of composition (in molar fractions) 0.15 Na_2O - 0.85 B_2O_3 referenced to that of vitreous B_2O_3.

vitreous B_2O_3. But two sites are clearly resolved (Fig. 23) in the ^{11}B NQR spectrum for this glass [2]. Clearly, the weaker response is lost under the strong resonance in the NMR recording. The stronger response arises from the boroxol groupings in the glass (see Fig. 7) but the origin of the second response has not yet been determined. As a metal oxide is added to B_2O_3, the type of ^{11}B NQR spectrum displayed in Fig. 24 is obtained. (The spectrum from pure B_2O_3 glass is superimposed for comparison.) In this glass containing 15 molar % Na_2O, there are several responses. One is apparently a reduced boroxol ring response and another may be an enlarged response from the second site in pure vitreous B_2O_3, but there is clearly a third response between those two and others may be present. A continuing program of identification of the responses, through comparison with the spectra from sodium borate compounds, is in progress along with an investigation of the effects of different thermal histories on the glass structure [2, 18].

[1] A. H. Silver and P. J. Bray, J. Chem Phys. **29,** 984 (1958).
[2] S. J. Gravina, PhD thesis, Brown University (1989).
[3] S. J. Gravina, P. J. Bray and G. L. Petersen, J. Non-Crystalline Solids **123,** 165 (1990).
[4] D. H. Lee, S. J. Gravina, and P. J. Bray, Z. Naturforsch. **45a,** 268 (1990).
[5] S. J. Gravina, and P. J. Bray J. Magnetic Resonance **89,** 515 (1990).
[6] P. J. Bray, Dong Hoon Lee, De Gen Mao, G. L. Petersen, S. A. Feller, D. L. Bain, D. A. Feil, Ponnappa Pandikuthira and Sumit Nijhawan, Z. Naturforsch. **47a,** 30(1992).
[7] P. J. Bray, S. J. Gravina, D. H. Hintenlang, and R. V. Mulkern. Magnetic Resonance Review, p. 263, Gordon and Breach Science Publishers, U. K. 1988.
[8] P. J. Bray, D. h. Lee, D. G. Mao, G. L. Petersen, S. A. Feller, D. L. Bain, D. A. Deil, P. Pandikutihra, and S. Nijhawan, "The Physics of Non-Crystalline Solids"; Ed. by L. David Pye, W. C. LaCourse, and H. J. Stevens, Taylor and Francis, London, Washington, DC, 1992, p. 713.
[9] G. H. Stauss, J. Chem Phys. **40,** 1988 (1964).
[10] H. M. Kriz, S. G. Bishop, and P. J. Bray, J. Chem Phys. **49,** 557 (1968).
[11] J. Krogh-Moe, Phys. Chem Glasses, **6,** 46 (1965).
[12] Yong-Hoon Yun, PhD thesis, Brown University (1978).
[13] R. Bersohn, J. Chem Phys. **20,** 1505 (1952).
[14] Degen Mao and Philip J. Bray, Solid State Nuclear Magnetic Resonance **1,** 255 (1992).
[15] Degen Mao, PhD thesis, Brown University (1991).
[16] R. B. Creel, J. Magn. Reson. **50,** 82 (1982).
[17] Degen Mao and Philip J. Bray, J. Non-Crystallogr. Solids **144,** 217 (1992).
[18] Prabhat K. Gupta, Ming L. Lui, and Philip J. Bray, J. Amer. Ceram. Soc. **68,** C-82 (1985).